Inorg. Chem. **2009**, *48*, 2626−2632

Electron Paramagnetic Resonance and Electron Nuclear Double Resonance Investigation of the Diradical Bis(α-iminopyridinato)zinc Complex

Maurice van Gastel,*,† Connie C. Lu, Karl Wieghardt, and Wolfgang Lubitz

Max-Planck-Institut für Bioanorganische Chemie, P.O. Box 101365, D-45413 Mülheim an der Ruhr, Germany

Received November 7, 2008

The neutral complex $Zn(L^{\bullet})_2$ and its monocationic analogue $[ZnL(L^{\bullet})\cdot THF]^{1+}$ have been previously reported to contain two and one monoanionic α-iminopyridinate$^{(1-)}$ π radical ligands, respectively [Lu, C.C.; Bill, E.; Weyhermüller, T.; Bothe, E.; Wieghardt, K. *J. Am. Chem. Soc.* **2008**, *130*, 3181−3197] (L represents the neutral α-iminopyridine form and THF is tetrahydrofuran). The electronic structures of these complexes have now been studied by Electron Paramagnetic Resonance (EPR) and Electron Nuclear Double Resonance (ENDOR) spectroscopy in conjunction with density-functional theory (DFT) calculations. The ENDOR spectra of the triplet $Zn(L^{\bullet})_2$ are characteristic of a localized diradical: these two ligand radicals exhibit dipolar exchange interactions, but no superexchange mechanism is operative, which would be consistent with its nearly tetrahedral coordination geometry. The monocationic species $[ZnL(L^{\bullet})\cdot THF]^{1+}$ ($S = 1/2$) has also been investigated by pulse EPR spectroscopy using large interpulse separations. It is shown that no radical hopping takes places on the time scale of the EPR experiment. The results obtained here, in particular the lack of asymmetry in the charge distribution between the two ligands in the triplet state, may be relevant for a better understanding of the electronic structure of naturally occurring diradicals and triplet states.

Introduction

Transition metal complexes featuring organic ligand radicals have recently received increased research interest.[1−6] An interesting application of such complexes is the use of redox-active ligands for the storage of electrons and/or holes. For example, Rauchfuss et al. have developed an Ir-based hydrogen-splitting catalyst in which the electrons from the hydrogen substrate are transferred to the redox non-innocent ligand during the catalytic cycle.[6] The use of redox-active organic molecules for electron transport is also highly relevant to processes in nature,[7−10] for example, those that are catalyzed by enzymes featuring amino acid radical.[7] Also, during photosynthesis, sunlight induces an electronic charge separation in which the excited electron travels over a multitude of cofactors (for example quinones and chlorophylls), in which the electron spin density resides on the organic part of the cofactor.

Though organic diradicals and even triradicals in frozen and liquid solutions have been studied extensively by magnetic resonance spectroscopy,[11] transition metal complexes featuring more than one redox non-innocent ligands are much less common. Recently, we have reported the preparation and characterization of a neutral bis(iminopyridinato)zinc complex $[Zn(L^{\bullet})_2]$ (Figure 1) and its cationic counterpart $[Zn(L)(L^{\bullet})]^{+}$, which both contain the monoan-

* To whom correspondence should be addressed. E-mail: vgastel@mpi-muelheim.mpg.de.

† Present address: Institut für Physikalische and Theoretische Chemie, Rheinische Friedrich-Wilhems-Universität Bonn, Wegeler Strasse 12, D-53115 Bonn, Germany.

(1) Hendrickson, D. N.; Pierpont, C. G. *Spin Crossover in Transition Metal Compounds II*; Springer: Berlin, London, 2004.
(2) Pierpont, C. G.; Lange, C. W. *Progress in Inorganic Chemistry*; John Wiley & Sons, Inc:: New York, 1994.
(3) Knijnenburg, Q.; Gambarotta, S.; Budzelaar, P. H. M. *Dalton Trans.* **2006**, 5442–5448.
(4) Ray, K.; Petrenko, T.; Wieghardt, K.; Neese, F. *Dalton Trans.* **2007**, 1552–1566.
(5) Blackmore, K. J.; Lal, N.; Ziller, J. W.; Heyduk, A. F. *J. Am. Chem. Soc.* **2008**, *130*, 2728–2729.
(6) Ringenberg, M. R.; Kokatam, S. L.; Heiden, Z. M.; Rauchfuss, T. B. *J. Am. Chem. Soc.* **2008**, *130*, 788–789.
(7) Stubbe, J.; van der Donk, W. A. *Chem. Rev.* **1998**, *98*, 705–762.
(8) Loew, G. H.; Harris, D. L. *Chem. Rev.* **2000**, *100*, 407–419.
(9) Whittaker, J. W. *Chem. Rev.* **2003**, *103*, 2347–2363.
(10) Kaim, W. *Dalton Trans.* **2003**, 761–768.
(11) Kurreck, H.; Kirste, B.; Lubitz, W. *Electron Nuclear Double Resonance Spectroscopy of Radicals in Solution*; VCH Publishers: Weinheim, Germany, 1988.

10.1021/ic802131w CCC: $40.75
Published on Web 02/10/2009

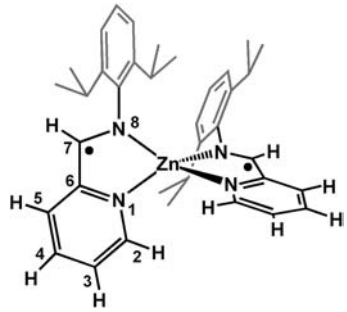

Figure 1. Schematic representation of the $Zn(L^{\bullet})_2$ complexes, including numbering scheme of the atoms.

Scheme 1. Overview of Oxidation States of the α-Iminopyridine Ligand

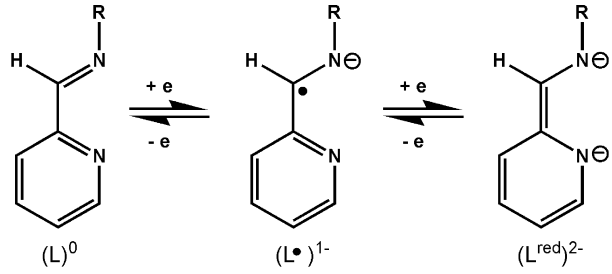

Scheme 2. Bacteriochlorophyll Dimer and $Zn(L)_2$ in the Neutral and Singly Oxidized Forms

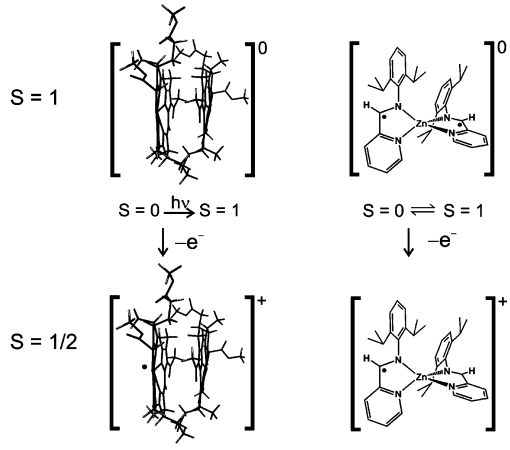

ionic ligand π radical $(L^{\bullet})^{-}$.[12] L represents the oxidized, neutral α-iminopyridine ligand. Its possible oxidation states are summarized in Scheme 1. We were intrigued by the possibility that these compounds may serve as functional models for metal-containing cofactors in nature that employ redox active ligands (e.g., porphyrins). For example, though geometrically and functionally different, the $[Zn(L^{\bullet})_2]$ and $[Zn(L)(L^{\bullet})]^{+}$ complexes display similarities on the electronic level to the bacteriochlorophyll dimer in the bacterial reaction center, which during the photosynthetic process may be present in the neutral singlet or triplet state or in the monocationic radical state (see Scheme 2).

Here, the Zn system is reinvestigated using advanced Electron Paramagnetic Resonance (EPR) methods with the aim of extracting a detailed picture of the spin density distribution of the ligand π radicals. We extend the characterization of the neutral triplet and cationic doublet Zn complexes using Electron Nuclear Double Resonance (ENDOR) spectroscopy and density-functional theory (DFT) calculations, both of which are ideally suited for investigating the wave function(s) of the unpaired electron(s). To our knowledge, this is the first time ENDOR spectroscopy has been applied to study spin densities in metal-coordination complexes that contain more than one ligand radical.

Materials and Methods

Samples of $Zn(L^{\bullet})_2$ and $[Zn(L)(L^{\bullet})][B(Ar_F)]_4$ (where Ar_F is 3,5-$(CF_3)_2(C_6H_3)$) were prepared anaerobically as described earlier. The $Zn(L^{\bullet})_2$ complex has been characterized by X-ray crystallography, susceptibility measurements, UV/vis, cyclic voltammetry, and continuous-wave (cw) EPR spectroscopy.[12] The geometry around the zinc center is approximately tetrahedral, with an angle ϑ between the two metal−ligand planes of 84(1)°. From magnetic susceptibility measurements a temperature-independent effective magnetic moment of 2.45 μ_B was deduced, which is indicative of essentially degenerate $S = 0$ and $S = 1$ ground states with minimal exchange interaction. The complex displays two nearby reversible oxidations at −1.33 and −1.16 V (vs Fc^{+}/Fc), which correspond to the oxidation of each ligand π radical. In this study, EPR samples of the neutral complex were dissolved in toluene.

The monocation $[Zn(L)(L^{\bullet})][B(Ar_F)]_4$ was previously characterized as a spin doublet based on a temperature-independent magnetic moment of 1.64 μ_B and an isotropic cw-EPR signal at $g = 2$.[12] Although the elemental analysis for the monocation is consistent with the formula $[Zn(L)(L^{\bullet})][B(Ar_F)]_4$, an X-ray diffraction study of a single crystal revealed the presence of one tetrahydrofuran (THF) solvent molecule coordinated to Zn, that is, $[Zn(L)(L^{\bullet})(THF)][B(Ar_F)]_4$. The angle ϑ between the two metal−ligand planes is drastically reduced to 47° because of the coordination of THF. Because the above salt is insoluble in toluene, the EPR samples discussed herein were dissolved in THF, a solvent in which it exists as the solvate-bound species $[Zn(L)(L^{\bullet})(THF)]^{+}$. The sample concentrations were about 1 mM.

Continuous-wave (cw) EPR measurements were performed on a Bruker E500 Elexsys X-band spectrometer equipped with an Oxford ESR910 flow cryostat and an ER4102ST rectangular cavity. Experimental conditions were $T = 30$ K, $\nu_{mw} = 9.457$ GHz, and $P_{mw} = 0.2$ mW. The pulsed EPR experiments at X-band were performed on a Bruker Elexsys E580 Fourier Transform EPR spectrometer. ESE-detected EPR spectra were measured with a two-pulse Hahn echo sequence in which the 90 degree pulse had a length of 16 ns. The time between the pulses was 312 ns.

ENDOR spectra were measured using the same spectrometer as that for the pulsed EPR measurements. In pulsed ENDOR spectroscopy one monitors the echo signal derived from the unpaired electron(s) while also applying a radiofrequency (RF) pulsed to induce an NMR transition.[13] When the RF frequency is such that a nuclear spin flip occurs, a change of the echo signal will be visible because the nuclear spin flip has changed the population distribution of the electron and nuclear spin energy levels.[14,15] Depending on how strongly this nuclear spin is coupled to the unpaired electron(s),

(12) (a) Lu, C. C.; Bill, E.; Weyhermüller, T.; Bothe, E.; Wieghardt, K. *J. Am. Chem. Soc.* **2008**, *130*, 3181−3197. (b) Trifonov, A. A.; Fedorova, E. A.; Borovkov, I. A.; Fukin, G. K.; Baranov, E. V.; Larionova, J.; Druzhkov, N. O. *Organometallics* **2007**, *26*, 2488−2491.

(13) Feher, G. *Phys. Rev.* **1959**, *114*, 1219–1244.

(14) Schweiger, A.; Jeschke, G. *Principles of Pulse Electron Paramagnetic Resonance*; Oxford University Press: Oxford, 2001.

(15) Carrington, A.; McLachlan, A. D. *Introduction to Magnetic Resonance*; Harper & Row: New York, 1967.

Scheme 3. Pulsed EPR Methods Used in This Work

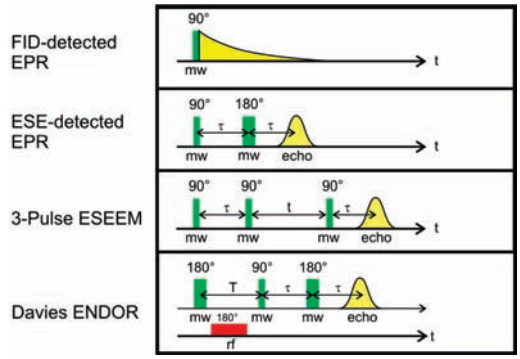

the nuclear spin flips occur at different RF frequencies. In this way, protons can be identified with weaker or stronger magnetic coupling to the electron spin.

Q-band EPR spectra were acquired on a Bruker Elexsys SuperQ Fourier Transform spectrometer equipped with an Oxford CF935 cryostat and a home-built resonator.[16,17] ESE-detected EPR spectra were recorded using a 40 ns - 440 ns - 80 ns Hahn echo pulse sequence. The FID measurements were performed with one soft microwave pulse with a length of 2000 ns. The pulse sequences used in this work are depicted in Scheme 3.

DFT calculations have been performed with the ORCA program package.[18] The input geometry for the neutral and cationic Zn complexes were derived from the respective crystal structures.[12] All DFT calculations were spin unrestricted calculations and employed the B3LYP functional. The triple-ζ TZV basis set of Ahlrichs[19] was used, augmented with polarization functions from the Turbomole library.[20] The self-consistent field (SCF) calculation was considered converged when the energy change was less than 10^{-8} Hartree (Eh), the change of elements of the density matrix less than 10^{-7} Eh, and the maximum element of the Direct Inversion of Iterative Subspace (DIIS) error less than 10^{-7} Eh. The geometry was converged with the following convergence criteria: change in energy $<10^{-5}$ Eh, average force $<5 \times 10^{-4}$ Eh/Bohr, and the maximum force $<10^{-3}$ Eh/Bohr. Nuclear hyperfine parameters were calculated using response theory by solving the coupled-perturbed SCF equations.[21] The coordinates of the atoms are included in the Supporting Information.

Theory. In this section, we introduce the relevant spin Hamiltonian parameters that were used to simulate the EPR and ENDOR spectra. In addition, the relationship between the hyperfine interaction parameters for the neutral triplet and the cationic doublet states is described.

Spin Hamiltonian Parameters. The spin Hamiltonian for two electron spins $\vec{s}_1$ and $\vec{s}_2$ coupled to nuclear spins $\vec{I}_i$ can be written as

$$\hat{H} = J\vec{s}_1 \cdot \vec{s}_2 + \vec{S} \cdot \vec{\vec{D}} \cdot \vec{S} + g_e \mu_B \vec{B} \cdot \vec{S} - \sum_{i=1}^{N} g_{n,i} \mu_N \vec{B} \cdot \vec{I}_i + \sum_{i=1}^{N} \vec{S} \cdot \vec{\vec{A}}_i \cdot \vec{I}_i + \sum_{i=1}^{N} \vec{I}_i \cdot \vec{\vec{Q}}_i \cdot \vec{I}_i \quad (1)$$

where the summations run over all nuclei with nuclear spin $I_i > 0$ coupled to the electron spin. The quantity $\vec{S}$ is the total electron spin, $\vec{\vec{D}}$ is the zero field tensor with principal values $-(1/3)D + E$, $-(1/3)D - E$, $+(2/3)D$,[22] μ_B and μ_N are the Bohr and nuclear magnetons, $g_{n,i}$ is the nuclear g value of the i-th nucleus, $\vec{\vec{A}}_i$ and $\vec{\vec{D}}_i$ are the nuclear hyperfine and quadrupole tensors for nucleus i. Quadrupole interaction only occurs for nuclei with $I > 1/2$ and thus are not relevant for simulating proton ENDOR spectra.

In a triplet system, the two important interactions between the two electrons are (a) the exchange interaction, J, and (b) the magnetic dipole interaction between the unpaired spins, which gives rise to zero field splitting (D, E). The exchange interaction originates from the Coulombic electron−electron repulsion and is responsible for the energy splitting between the triplet and singlet states. The sign of J determines whether the low-spin state ($J > 0$) or the high-spin state ($J < 0$) is the ground state. When J is small (<2 cm^{-1}), it becomes non-trivial to determine the magnitude of J exactly, although the sign of J should be easier to extract using low-temperature measurements.

The magnetic dipole interaction essentially determines the shape of the EPR spectrum. If the two unpaired electrons are far away from each other so that they are uncoupled, then the resultant spectrum would simply be a superposition of the two doublet EPR spectra. In the other extreme, when the spin−spin interaction is large (large zero field splitting), the system has to be described as a triplet state, and no EPR signal can be observed at room temperature because of the fast relaxation time of the electron spins. For the case of intermediate coupling (diradicals), the EPR signal would be observable at room temperature and would broaden because of dipole−dipole coupling. Additionally, a triplet state gives a characteristic half-field signal owing to the $\Delta M_S = 2$ transition. A more extensive description is given elsewhere.[11]

For organic radicals the g tensor can be well approximated by an isotropic g value, equal to that of the free electron $g_e = 2.0023$. The zero field splitting give rises to a splitting of the M_S sublevels even in zero magnetic field. The parameter D defines the magnitude of the zero field splitting, the parameter E the rhombicity, and E/D is called the asymmetry parameter ($|E/D| < 1/3$).

Hyperfine Interaction and ENDOR Resonance Condition in a Monoradical and a Diradical. The isotropic hyperfine interaction for protons in the equatorial plane of the π system of an aromatic molecule is derived from spin polarization.[15] For a C−H fragment, the unpaired electron in the $2p_z$ orbital at C interacts via the exchange interaction with the α electron of the C−H σ bond, but not with the β electron. This polarizes the C−H σ bond and gives rise to negative spin density at the proton.[15]

For an electron spin $S = 1/2$, as is the case for $[ZnL(L^{\bullet})\cdot THF]^{1+}$, coupled to a nuclear spin $I = 1/2$, for example, a proton nuclear spin, the energy level scheme is given in Figure 2a. The nuclear spin transitions are determined by terms 4 and 5 of eq 1 and occur at

(16) Sinnecker, S.; Reijerse, E.; Neese, F.; Lubitz, W. *J. Am. Chem. Soc.* **2004**, *126*, 3280–3290.
(17) Silakov, A.; Reijerse, E. J.; Albracht, S. P. J.; Hatchikian, E. C.; Lubitz, W. *J. Am. Chem. Soc.* **2007**, *129*, 11447–11458.
(18) Neese, F. *ORCA - An ab initio, Density Functional and Semiempirical program package*, Version 2.6, revision 63; Rheinische Friedrich-Wilhelms-Universität Bonn: Bonn, Germany, 2008.
(19) Schaefer, A.; Horn, H.; Ahlrichs, R. *J. Chem. Phys.* **1992**, *97*, 2571–2577.
(20) Turbomole Basis set library, available at ftp.chemie.uni-karlsruhe.de/pub/basen, 2008.
(21) Neese, F. *J. Chem. Phys.* **2003**, *118*, 3939–3948.
(22) Atherton, N. M. *Principles of Electron Spin Resonance*; Ellis Horwood Limited: Chichester, 1993.
(23) Hoffman, B. M. *J. Phys. Chem.* **1994**, *98*, 11657–11665.

$$\nu^{D}_{ENDOR} = \nu_n \pm \frac{A_D}{2} \quad (2)$$

where ν_n is the nuclear Zeeman frequency and A_D the effective hyperfine interaction in the doublet state. Corrections to this equation may be necessary when $\nu_n \pm (A_D)/(2)$ becomes close to 0 MHz and the anisotropy of the hyperfine interaction is large. For a monoradical, the ENDOR spectrum is symmetric about the Zeeman frequency. For a diradical state $Zn(L^{\bullet})_2$, the energy level diagram shown in Figure 2b indicates that the EPR $M_S = 0 \leftrightarrow \pm 1$ transitions gives rise to ENDOR signals at

$$\nu^{T}_{ENDOR} = \nu_n - M_S A_T \quad (3)$$

The quantity A_T represents the hyperfine interaction in the triplet state. From this formula, is is clear that the ENDOR spectrum of the diradical is only symmetric if the $M_S = 0 \leftrightarrow +1$ and $M_S = 0 \leftrightarrow -1$ transitions contribute equally at the selected magnetic field position. If the diradical is comprised of two identical monoradicals, the hyperfine interaction of the diradical, A_T, equals half of the hyperfine interaction of the monoradical A_D,

$$A_T = \frac{A_D}{2} \quad (4)$$

Thus, if one inserts eq 4 in eq 3, the frequencies present in the ENDOR spectrum of the diradical spectrum are the same as those for the monoradical, given by eq 2.

The Davies ENDOR spectra of the doublet monoradical and triplet diradical were simulated using a home written program that numerically calculates the energy level diagram of the electron spin and nuclear spin using the Hamiltonian of eq 1 and assuming a Boltzman distribution of the population. Analytical expressions are also available,[23] though for the system under investigation it turned out that a numerical procedure is more efficient. The ZFS parameter E was set to 0 cm^{-1}. The orientation average necessary to calculate the pulsed EPR and Davies ENDOR spectrum of the powder sample

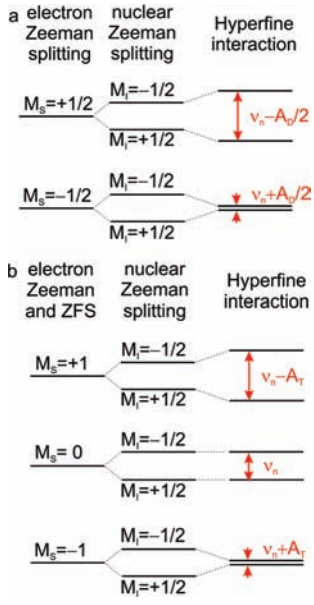

Figure 2. Energy level diagram for a nuclear spin $I = 1/2$ coupled to (a) an electron spin $S = 1/2$ and (b) and electron spin $S = 1$ with $A_{D,T} < 0$. Note that for the triplet state, the signals at high frequency ($\nu_n - A_T$) will be attenuated because of the presence of the singlet state near the $M_S = +1$ level (see Figure 4).

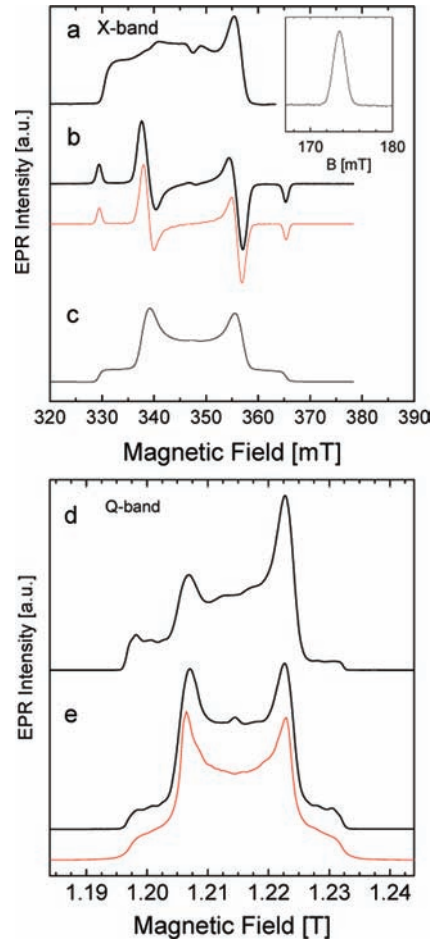

Figure 3. (a) X-band ESE-detected EPR spectrum and (b) cw EPR spectrum (black) and simulation (red) of $Zn(L^{\bullet})_2$. Experimental conditions: (a) $T =$ 10 K, $\nu_{mw} = 9.75$ GHz, length of 90 degree pulse 16 ns, $\tau = 312$ ns. (b) $T = 30$ K, $\nu_{mw} = 9.457$ GHz, $P_{mw} = 0.2$ mW. (c) Integral of (b). (d) Q-band two pulse EPR spectrum of neutral $Zn(L^{\bullet})_2$. (e) FID detected EPR spectrum (black) and simulation (red). Experimental conditions: $T = 10$ K, $\nu_{mw} =$ 34.050569 GHz, Hahn echo sequence 40 ns - 440 ns - 80 ns, FID pulse 2 μs. The half-field signal is shown as an inset in Figure 3a. In the center of the EPR spectra, a small contribution of a radical species ($S = 1/2$) is present. The cw EPR spectra (b) have been scaled to 9.75 GHz for easy comparison with the ESE-detected spectrum.

was performed using principal axes system of the ZFS tensor as a reference. The ENDOR transitions of the doublet system and of the $M_S = \pm 1$ levels of the triplet system were dressed with a Gaussian of width 1.1 MHz to simulate hyperfine strain. Since the nuclear-spin transitions of the $M_S = 0$ level are not susceptible to hyperfine strain, they were assigned a smaller line width of 0.2 MHz.

Results and Discussion

EPR of $Zn(L^{\bullet})_2$ and $[ZnL(L^{\bullet})\cdot THF]^{1+}$. Continuous wave and ESE-detected EPR spectra of $Zn(L^{\bullet})_2$ recorded at X-band microwave frequencies are shown in Figure 3. The cw EPR spectrum displays a triplet EPR signal typical for two radicals coupled by dipolar spin−spin interaction (Figure 3b). The spectrum has been well simulated with a D value of $|D| =$ 488 MHz (0.0163 cm^{-1}). The E parameter is negligibly small. This is expected for a simple model if one considers a tetrahedral coordination geometry of Zn whereby the spin densities of the nitrogen atoms of both bidentate radicals are approximated by point spins.[15] The D value agrees with other

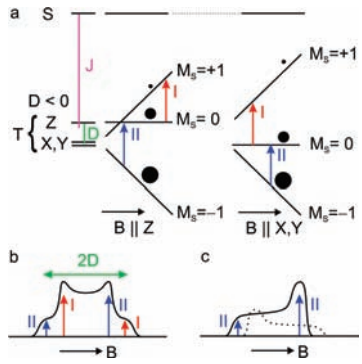

Figure 4. (a) Energy level diagram for the triplet (T) ground-state and singlet (S) excited state, separated by the exchange interaction J. The triplet sublevels are already split without a magnetic field by the zero-field parameter D. Upon switching on the magnetic field, the triplet sublevels split further into the $M_S = 0, \pm 1$ sublevels. EPR transitions are indicated with red and blue arrows. Thermal population of the triplet sublevels are indicated by balls of different size. (b) Idealized ESE-detected EPR spectrum in which the $M_S = 0 \leftrightarrow +1$ (I) and $M_S = 0 \leftrightarrow -1$ (II) transitions contribute equally. (c) ESE-detected EPR spectrum with shortened phase memory time for the $M_S = 0 \leftrightarrow +1$ transition only. Note the asymmetric EPR spectrum occurring in this case.

analogous $Zn(L^{\bullet})_2$ systems that feature two alpha-diimine ligand radicals.[24,25] In this work by Gardiner, the triplet EPR spectrum was successfully modeled with a small zero-field splitting of 0.0231 cm^{-1}.[24] A room temperature spectrum was also observed, thus classifying this class of compounds as weakly coupled diradicals.[24]

Strikingly, the ESE-detected EPR spectrum (Figure 3a) does not resemble the integral of the cw EPR spectrum (Figure 3c). No signal is observed between at magnetic field settings above 358 mT, and the echo amplitude at field below 358 mT is strongly modulated owing to the electron spin echo envelope modulation (ESEEM) effect and not characteristic for two dipolarly coupled radicals. An ESE-detected signal at half-field was observed, which is shown in the inset of Figure 3a, which also characterizes this system as an $S = 1$ triplet diradical.

At Q-band microwave frequencies, the ESEEM effect is less pronounced than at X-band. The ESE-detected EPR spectrum (Figure 3d) now resembles that of a weakly coupled diradical system and has the same width as the cw EPR spectrum recorded at X-band (Figure 1a), but one of the two branches of the double Pake pattern is attenuated by a factor of 2. Only with FID detection, the Q-band EPR spectrum (Figure 3e) displays a double Pake pattern with branches of equal intensity. The spectrum has been simulated using the same D value as determined from the cw EPR spectrum at X-band.

The discrepancy between cw and FID detection on one side and ESE detection on the other side is striking and unusual. Two effects play a role. First, the width of the EPR spectrum is much larger than the width of the excitation pulse, giving rise to a complicated oscillatory FID signal that depends on the pulse length and its excitation bandwidth.[14] Second, relaxation times play a role, as can be seen in the energy level diagram associated with the diradical $Zn(L^{\bullet})_2$, shown in Figure 4a. The system has been characterized as a triplet ($S = 1$) ground-state in which both ligands carry one unpaired electron.[12] Though the absolute sign of D cannot be determined from experiment, it is likely negative, since the ligands are far enough away so that the spin−spin coupling resembles that of two weakly coupled point electron spins for which D is negative.[15] Under these conditions and without consideration of the singlet state, two Pake patterns, indicated by I and II in Figure 4 are expected. They correspond to the $M_S = 0 \leftrightarrow +1$ and $M_S = 0 \leftrightarrow -1$ transitions of the triplet manifold. An idealized EPR spectrum is shown in Figure 4b, which resembles the FID detected spectrum in Figure 3e and the integral of the cw EPR spectrum in Figure 3b. For very small values of J, the presence of the singlet state near the $M_S = +1$ triplet sublevel becomes important and will shorten the phase memory time of transition I, which can result in an attenuated amplitude and even a complete disappearance of the corresponding Pake pattern. Under such conditions, the intensity distribution of the EPR spectrum becomes asymmetric, as is indicated schematically in Figure 4c, which resembles the ESE-detected EPR spectra shown in Figures 3a and 3d. It is clear that the asymmetry is method-related, and it is of minor importance for the understanding of the electronic structure of $Zn(L^{\bullet})_2$. Thus, the observation of a triplet EPR signal, a half-field signal, and the degree of asymmetry in the ESE-detected spectra are compatible with the absence of any superexchange,[15] which usually dominates the exchange interaction. Then, only the through-space Coulomb contribution to the exchange interaction remains, giving rise to a small J coupling on the order of the microwave quantum.

The EPR spectrum of the cation $[ZnL(L^{\bullet})\cdot THF]^{1+}$ is typical of an organic radical. It is characterized by a structureless signal with a width of about 75 MHz as is shown in the inset of Figure 5a. No proton hyperfine structure is observed, which indicates that these interactions are hidden in the EPR line width and that more advanced EPR methods are required to extract information about these interactions.

ENDOR of $Zn(L^{\bullet})_2$ and $[ZnL(L^{\bullet})\cdot THF]^{1+}$. Further investigations of the electronic structure of $Zn(L^{\bullet})_2$ and $[ZnL(L^{\bullet})\cdot THF]^{1+}$ have been performed by Davies ENDOR spectroscopy. With this technique, the magnetic interaction between the electron and nuclear spins, that is, the hyperfine interaction, can be determined. The ENDOR spectrum for $[ZnL(L^{\bullet})\cdot THF]^{1+}$ is shown in Figure 5a. Given the excitation bandwidth of the microwave pulses of about 0.6 mT (17 MHz), virtually no orientation selection is achieved at X-band frequency, and all possible orientations of the molecule with respect to the magnetic field contribute to the ENDOR spectrum. This powder ENDOR spectrum spans the entire accessible RF range from 1 to 32 MHz and displays broad and poorly resolved bands positioned symmetrically around the proton Zeeman frequency, $\nu_n(^1H) = 14.73$ MHz for a field setting of 346.0 mT. In total, three intensity maxima are found in the frequency region below $\nu_n(^1H)$, as well as the region above. Those below occur at about 4, 9, and 12

(24) Gardiner, M. G.; Hanson, G. R.; Henderson, M. J.; Lee, F. C.; Raston, C. L. *Inorg. Chem.* **1994**, *33*, 2456–2461.
(25) Rijnberg, E.; Richter, B.; Thiele, K. H.; Boersma, J.; Veldman, N.; Spek, A. L.; van Koten, G. *Inorg. Chem.* **1998**, *37*, 56–63.

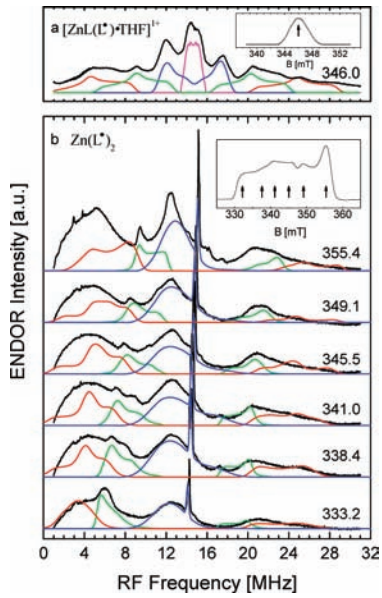

Figure 5. (a) X-band Davies ENDOR spectrum of the radical cation $[ZnL(L^{\bullet})\cdot THF]^{1+}$ with $S = 1/2$. (b) Orientation selected Davies ENDOR spectra of the neutral diradical $Zn(L^{\bullet})_2$. The ESE-detected EPR spectra are shown as insets in (a) and (b). The magnetic field settings [mT] at which the ENDOR spectra are recorded are indicated in the figure and by arrows in the EPR spectra. Experimental conditions: $T = 10$ K, RF pulse length 8 μs, microwave pulses 112 ns - 56 ns - 112 ns, $\nu_{mw} = 9.75$ GHz.

MHz, corresponding to effective hyperfine couplings of 21.5, 11.5, and 5.5 MHz, as calculated by eq 2.

For $Zn(L^{\bullet})_2$, orientation selection is obtained with respect to the dominant zero-field splitting in the EPR spectrum. Orientation-selected ENDOR spectra for $Zn(L^{\bullet})_2$ are shown in Figure 5b. A narrow signal at the proton Zeeman frequency is visible in all spectra, which corresponds to the transition at ν_n ($M_S = 0$), see eq 3. The broad signals at frequencies lower than $\nu_n(^1H)$ display a striking resemblance to those in the ENDOR spectrum of $[ZnL(L^{\bullet})\cdot THF]^{1+}$. The amplitude of the signals above $\nu_n(^1H)$ is attenuated with respect to those of $[ZnL(L^{\bullet})\cdot THF]^{1+}$. The reduced intensity of the high-frequency signals is in line with the attenuated amplitude of the high-field peak pattern in the ESE-detected EPR spectrum (Figure 3a).

The observation of essentially identical ENDOR spectra for the triplet $Zn(L^{\bullet})_2$ and the doublet $[ZnL(L^{\bullet})\cdot THF]^{1+}$ is striking and in-line with a diradical composed of two identical monoradicals, described in the Theory section. In such a case, the hyperfine interaction of the triplet state, A_T, equals half of the hyperfine interaction of the doublet state A_D. Thus the relation $A_T = (A_D)/(2)$ is characteristic for a delocalized diradical triplet state in which the two radicals are localized on their respective ligands.

Simulations and DFT Calculations. In principle, ENDOR signals can be observed for ^1H ($I = 1/2$) and ^{14}N ($I = 1$). However, since the nitrogen atoms carry a large part of the spin density (vide infra) and are characterized by highly anisotropic hyperfine couplings, the signals are broadened and virtually undetectable in case of the doublet $[ZnL(L^{\bullet})\cdot THF]^{1+}$. In the triplet $Zn(L^{\bullet})_2$, only the ^{14}N transition frequencies from the $M_S = 0$ are observable in the low-frequency part of the ENDOR spectrum. These frequencies are also broad and unresolved because of the quadrupole interaction, as well as the presence of four nitrogen nuclei. The ENDOR technique thus does not provide hyperfine information for ^{14}N, and the nuclear spin of the nitrogen atoms is not a suitable reporter for investigation of the wave function of the unpaired electron (see also Supporting Information). We therefore concentrated on elucidation of the ^1H hyperfine coupling constants.

Table 1. Isotropic and Anisotropic Proton Hyperfine Coupling Constants [MHz] for $[ZnL(L^{\bullet})\cdot THF]^{1+}$ and $Zn(L^{\bullet})_2$ as Determined from ENDOR Experiments and DFT Calculations[a]

		$[ZnL(L^{\bullet})\cdot THF]^{1+}$				$Zn(L^{\bullet})_2$	
atom		experiment	DFT	atom		experiment	DFT
H7	a_{iso}	−20.0	−18.7	H7,H7′	a_{iso}	−10.0	−9.4
	A'_{xx}	8.5	14.5		A'_{xx}	4.1	6.9
	A'_{yy}	−0.2	−0.2		A'_{yy}	−0.1	−1.5
	A'_{zz}	−8.3	−14.3		A'_{zz}	−4.0	−5.3
H3	a_{iso}	−11.3	−9.7	H3,H3′	a_{iso}	−5.9	−6.1
	A'_{xx}	7.3	7.7		A'_{xx}	3.1	4.1
	A'_{yy}	0.2	0.2		A'_{yy}	−0.1	−0.6
	A'_{zz}	−7.5	−7.9		A'_{zz}	−3.0	−3.5
H4	a_{iso}	−4.2	−3.2	H4,H4′	a_{iso}	−2.1	−2.0
	A'_{xx}	3.9	3.9		A'_{xx}	1.9	2.2
	A'_{yy}	−1.0	−1.0		A'_{yy}	−0.5	−0.8
	A'_{zz}	−2.9	−2.9		A'_{zz}	−1.4	−1.4
H5	a_{iso}	−4.2	−3.3	H5,H5′	a_{iso}	−2.1	−1.9
	A'_{xx}	3.9	2.8		A'_{xx}	1.9	1.7
	A'_{yy}	−1.0	−0.7		A'_{yy}	−0.5	−0.3
	A'_{zz}	−2.9	−2.1		A'_{zz}	−1.4	−1.4

[a] For numbering of the atoms, see Figure 1. The DFT calculations for $Zn(L^{\bullet})_2$ give the same couplings for equivalent protons of both radicals to within 0.1 MHz.

Simulations of the ENDOR spectra have been included in Figure 5. Given the low resolution of the signals, initial parameters for the simulations were taken from DFT calculations (vide infra). The ENDOR spectra for $[ZnL(L^{\bullet})\cdot THF]^{1+}$ have been simulated by four sets of protons. The proton with largest coupling, indicated in red, corresponds to position H7, the proton of second largest coupling is indicated in green and is located at position H3, and the blue part of the simulation corresponds to two protons H4 and H5 (cf. Figure 1). In addition, the center part of the ENDOR spectrum, where protons of weaker coupling contribute, has been simulated by an effective proton hyperfine interaction of 0.5 MHz, indicated in magenta. The simulation agrees well with experiment and the optimized hyperfine coupling constants, which only slightly differ from those of the DFT calculations, are included in Table 1.

The orientation-selected Davies ENDOR spectra have been simulated by the same set of three protons. Since the width of the triplet EPR spectrum (Figure 3) of $Zn(L^{\bullet})_2$ is larger than the excitation bandwidth of the microwave pulses, orientation selection becomes important and small changes of the features in the ENDOR spectra are observed at different positions in the ESE-detected EPR spectrum. Optimized parameters for the protons in $Zn(L^{\bullet})_2$ are included as well in Table 1. The signals on the high-frequency side have been scaled down in amplitude to account for the decreased amplitude of the $M_S = 0 \leftrightarrow +1$ transition in the ESE-detected EPR spectrum.

Nuclear hyperfine coupling constants from DFT calculations for $Zn(L^{\bullet})_2$ and $[ZnL(L^{\bullet})\cdot THF]^{1+}$ are also included in Table 1. The hyperfine coupling constants after optimization

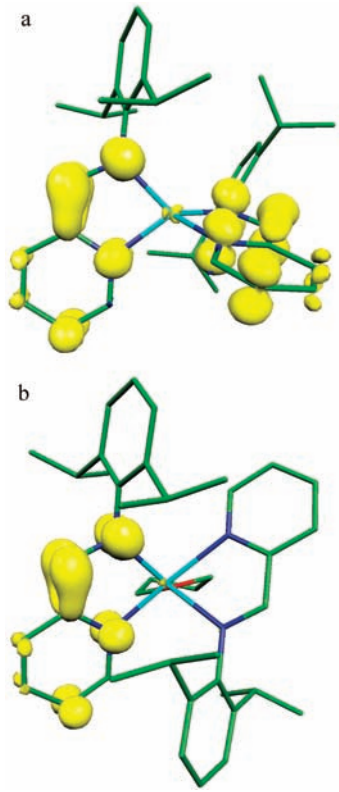

Figure 6. Spin density plots for (a) the neutral diradical $Zn(L^{\bullet})_2$ and (b) the radical cation $[ZnL(L^{\bullet})\cdot THF]^{1+}$.

accurately describe the signals observed in the ENDOR spectrum for both the neutral diradical and the radical cation complex. Particular mismatches concern the low-frequency region (0−6 MHz) of the ENDOR spectra of $Zn(L^{\bullet})_2$. The mismatch likely stems from the hyperfine interactions of the four nitrogen atoms that also contribute to this frequency region. The calculations confirm the localized radical character, since the hyperfine couplings for $Zn(L^{\bullet})_2$ are about half the value of those for $[ZnL(L^{\bullet})\cdot THF]^{1+}$. The spin density distribution is given in panels a and b of Figure 6 for $Zn(L^{\bullet})_2$ and $[ZnL(L^{\bullet})\cdot THF]^{1+}$, respectively. In the radical cation, essentially all spin density is located on one radical (Figure 6b). In the neutral, diradical complex, the second ligand now carries spin density as well, which has an identical distribution as the spin density of the cation (Figure 6a). The ligand atoms that carry the largest spin density are summarized in Table 2. Most spin density (48%) is found in the N8−C7 bond. The pyridine moiety carries 43% spin density. The metal carries only 1.8% spin density. The Löwdin spin densities at the protons H3, H6, H4, and H5 are also included in the table. They compare very well with the spin densities estimated from the isotropic hyperfine interaction according to $\rho_{exp} = a_{iso}/1419$ MHz,[15] again confirming the accurate description of localized mono- and diradicals by the DFT calculation.

Table 2. Löwdin Spin Density Distribution ρ [%] of the ligand radical $L^{\bullet}$ as Derived from the DFT Calculations of $[ZnL(L^{\bullet})\cdot THF]^{1+}$ and $Zn(L^{\bullet})_2$[a]

atom	ρ	atom	ρ	ρ_{exp}
N8	23.0			
C7	24.9	H7	−0.0073	−0.0070
C6	7.3			
N1	14.9			
C4	4.2	H4	−0.0016	−0.0015
C5	4.2	H5	−0.0016	−0.0015
C3	12.9	H3	−0.0050	−0.0042
		H2	−0.0002	

[a] For numbering of the atoms, see Figure 1. In case of the protons, the last column contains the experimentally determined spin density, $\rho_{exp} = a_{iso}/1419$ MHz.[15] The total spin density is normalized to the number of unpaired electrons of the system (i.e., 1 for the monoradical and 2 for the diradical).

Conclusion

The triplet $Zn(L^{\bullet})_2$ and doublet $[ZnL(L^{\bullet})\cdot THF]^{1+}$ complexes have been investigated by EPR and ENDOR spectroscopy and DFT calculations. It was found that the redox active part of the molecule is the ligand. ENDOR spectroscopy revealed that the triplet state $Zn(L^{\bullet})_2$ ($S = 1$) contains two ligand radicals that interact by magnetic dipole−dipole interaction. The observation of an EPR signal of a triplet state indicates that superexchange mechanisms, which give rise to large exchange interaction and favor the singlet state, are quenched.

The ENDOR spectra of the neutral and singly oxidized complex display essentially the same signals, indicating that no asymmetry is present between the ligand radicals in the neutral state, and that an electron is selectively removed from one of the ligands upon single oxidation. These results are fully supported by DFT calculations. The observation of pulse EPR signals for $[ZnL(L^{\bullet})\cdot THF]^{1+}$ with interpulse separations of up to 50 μs implies that the phase memory time is longer than 50 μs. This means that radical hopping, if present at all in $[ZnL(L^{\bullet})\cdot THF]^{1+}$, does not occur on the time scale accessible by EPR spectroscopy.

Acknowledgment. The authors thank Dr. Eckhard Bill for carefully reading the manuscript. This work was supported financially by the Max-Planck Gesellschaft and DFG Projekt (GA 1100/1−2). C.C.L. thanks the Alexander von Humboldt Foundation for a postdoctoral fellowship.

Supporting Information Available: Orientation-selected Q-band ESEEM spectra of $Zn(L^{\bullet})_2$ and calculated ^{14}N hyperfine coupling constants. Coordinates [Å] of the models used in the DFT calculations. This material is available free of charge via the Internet at http://pubs.acs.org.

IC802131W